# The Myb/SANT domain of the telomere-binding protein TRF2 alters chromatin structure

Asmaa M. Baker[1], Qiang Fu[2], William Hayward[1], Stuart M. Lindsay[2] and Terace M. Fletcher[1],*

[1]Department of Biochemistry and Molecular Biology, University of Miami Miller School of Medicine, Miami, FL 33101-6129 and [2]Department of Chemistry and Biochemistry, Arizona State University, Tempe, AZ 85287, USA

## ABSTRACT

**Eukaryotic DNA is packaged into chromatin, which regulates genome activities such as telomere maintenance. This study focuses on the interactions of a myb/SANT DNA-binding domain from the telomere-binding protein, TRF2, with reconstituted telomeric nucleosomal array fibers. Biophysical characteristics of the factor-bound nucleosomal arrays were determined by analytical agarose gel electrophoresis (AAGE) and single molecules were visualized by atomic force microscopy (AFM). The TRF2 DNA-binding domain (TRF2 DBD) neutralized more negative charge on the surface of nucleosomal arrays than histone-free DNA. Binding of TRF2 DBD at lower concentrations increased the radius and conformational flexibility, suggesting a distortion of the fiber structure. Additional loading of TRF2 DBD onto the nucleosomal arrays reduced the flexibility and strongly blocked access of micrococcal nuclease as contour lengths shortened, consistent with formation of a unique, more compact higher-order structure. Mirroring the structural results, TRF2 DBD stimulated a strand invasion-like reaction, associated with telomeric t-loops, at lower concentrations while inhibiting the reaction at higher concentrations. Full-length TRF2 was even more effective at stimulating this reaction. The TRF2 DBD had less effect on histone-free DNA structure and did not stimulate the t-loop reaction with this substrate, highlighting the influence of chromatin structure on the activities of DNA-binding proteins.**

## INTRODUCTION

Eukaryotic chromosomes are assembled into chromatin structures comprised of core histones and other architectural proteins. Central to chromatin structure is the arrangement of the nucleosome core, which has four pairs of small, basic histones to form the core octamer, wrapped within 1.67 left-handed superhelical DNA turns (1). This special arrangement of nucleosomal DNA within nucleosomal fibers sets up a specific binding substrate for many DNA-binding factors and chromatin architectural proteins (2). Although it has been shown that nucleosomes affect the binding of several factors, the influence of these factors on the structure of nucleosomal array fibers is less studied.

One region of the genome where chromatin structure has an influence on function is the telomere (3). Telomeres are specialized nucleoprotein complexes assembled on repetitive, guanine-rich DNA which function to protect chromosome ends from being recognized and processed as double-stranded DNA breaks. Mammalian telomeres possess periodically spaced nucleosomes with relatively short spacing of $\sim$160 bp (4,5), an organization that extends to the very end of the telomere (6). Additionally, linker histones (H1) were detected in telomeric chromatin (4), and H1-depletion in mice increases telomere length (7). Mammalian telomere length maintenance is also regulated by trimethylated lysine 9 of histone H3 and lysine 20 of histone H4, along with the presence of heterochromatin protein 1 subtypes (8). The relationship of hallmark features of heterochromatin and telomere length suggests key roles of mammalian telomeric chromatin structure in proper function.

Mammalian telomeres possess a tandemly repeated, 5′-TTAGGG-3′ DNA sequence which is maintained by telomerase (9). Telomere integrity is also preserved by a specific telomere nucleoprotein complex (10,11) referred to as shelterin (12). A key player in the shelterin complex is TTAGGG repeat factor 2, TRF2. Cells expressing a dominant negative TRF2 undergo cellular senescence or apoptosis mediated by p53/ATM (13). Telomere dysfunction induced by dominant negative TRF2 expression results in chromosome end-to-end fusions and a reduction of the G-strand overhang (14). Overexpression of TRF2

*To whom correspondence should be addressed. Tel: +1 305 243 6297; Fax: +1 305 243 3955; Email: tfletcher@med.miami.edu

triggers telomere shortening; however, cells with these shortened telomere lengths appear to be protected from senescence (15).

In addition to its role in the shelterin complex, TRF2 has been shown to stabilize looped higher-order structures, which are thought to sequester the G-strand overhang from degradation and DNA damage signaling (16–18). Both TRF2 and another shelterin protein, TRF1, interact with telomeric DNA sequence through a myb/SANT DNA-binding domain (19). This DNA-binding domain was shown to be important for interactions of TRF2 with telomeric chromatin *in vivo*; a temperature sensitive mutation in this domain disrupted the shelterin complex and rendered telomeres dysfunctional (20). These interactions occur mainly through the C-terminal helix within the DNA major groove, while an N-terminal extension interacts with the minor groove (19). Consequently, it is possible that binding to DNA sites may be hindered in nucleosomes; an important consideration if the binding substrate is nucleosomal chromatin. TRF1 has been found to bind to telomeric chromatin (21), but no detailed analysis on the interactions of TRF2 and TRF1 with nucleosomal fibers have been published to date. Nevertheless, TRF1 and the yeast ortholog, Rap1p, have been shown to interact with mononucleosome cores, while binding is inhibited when binding sites are situated near the nucleosome dyad (22,23). Furthermore, TRF1 has a strong preference for sites facing outward from the nucleosome and these interactions produced DNase I hypersensitive regions, suggesting that it alters nucleosome structure. Despite this, no histone dissociation was observed, suggesting that TRF1 and, by extension, TRF2 may have specific requirements for interacting with nucleosomal fibers and potentially altering their global structure. Currently, no information exists explaining how myblike DNA-binding domains interact with and affect nucleosomal array fibers, which is particularly important considering the finding that telomeric chromatin has been shown to be in the form of t-loops (21).

This study represents a structural characterization of the interactions of the TRF2 myb/SANT DNA-binding domain (TRF2 DBD) interacting with its sites within a nucleosomal array fiber. Although effects on global chromatin structure are difficult to recapitulate *in vitro*, this study takes advantage of the fact that telomeric DNA provides a tandem array of many factor-binding sites which essentially amplify subtle structural changes. In addition, the key to analysis of factor binding to complicated nucleosomal fiber assemblies in solution is the use of an analytical agarose gel electrophoretic (AAGE) technique which provides parameters associated with the surface electrical charge density, hydrodynamic radius and conformational flexibility of these assemblages (24,25). This method was successful in revealing previously unknown structural characteristics of chromatin reconstituted *in vitro* (24,26–29) and isolated from cells (30). Interpretation of nucleosomal fiber structures analyzed by AAGE in the present study was facilitated by imaging single molecules with atomic force microscopy. The data show that the TRF2 myb/SANT DNA-binding domain (TRF2 DBD) had the ability to access its sites within

nucleosomal arrays and alter their structure, resulting in a reduction in negative surface charge concomitant with an increase in effective radius. Unique to this approach was the ability to observe that the TRF2 DBD increased the flexibility of nucleosomal arrays when added at low concentrations. The increase in fiber radius and flexibility caused by lower concentrations of TRF2 DBD coincided with an increase in the ability of these fibers to interact with a single-stranded $5'$-d(TTAGGG)$_7$-$3'$ oligonucleotide in a reaction associated with t-loop formation (31). In contrast, addition of higher concentrations of the TRF2 DBD did not cause a further increase in radius but did continue to reduce the negative surface charge, flexibility and access of micrococcal nuclease. At these higher concentrations, the TRF2 DBD inhibited the reaction of nucleosomal arrays with the single-stranded oligonucleotide. These results suggest that TRF2 may influence telomere function by modulating chromatin structure.

## MATERIALS AND METHODS

### Materials

The 3.5-kb pRST5 plasmid (17) contains ∼96 TTAGGG DNA repeats. The plasmid was digested with PvuII to liberate a 1-kb fragment containing the telomeric DNA and 2.5-kb non-telomeric DNA (Figure 1A). Alternatively, the plasmid was digested to liberate a ∼2-kb fragment containing the telomeric DNA with a ∼1-kb and two ∼220-bp fragments of non-telomeric DNA. The telomeric DNA was situated approximately in the center of the 1- and 2-kb fragments. The p208-12 plasmid (32) contains 12 repeats of the *Lytechinus* 5S rDNA that positions nucleosomes and the 2.5-kb, 208-12 fragment is liberated by HhaI digestion. Fragments containing telomeric DNA were either gel purified using Qiagen QIAXII gel extraction kit or were left unpurified allowing for non-telomeric DNA to be used as an internal control for the AAGE analysis. For atomic force microscopy (AFM) studies, the pRST5 plasmid was digested with SfaNI and the 2-kb fragment with the telomeric region was separated on a 0.8% agarose gel. The fragment was excised, electroeluted and concentrated with an 8000-kDa filter (Amicon, Millipore), followed by phenol–chloroform extraction and ethanol precipitation.

Recombinant, His6-tagged TRF2 DBD was expressed in *E. coli* BL21 cells (Invitrogen) and purified using Talon Co$^{2+}$ (Clontech) beads (33). Recombinant, His6-tagged full-length TRF2 was baculovirus expressed in Sf9 cells and purified as previously described (34).

### Reconstitution of nucleosomal arrays

Histone octamers were purified from HeLa cells (35) or chicken erythrocytes (32). Nucleosomal arrays were reconstituted by polyglutamate transfer or stepwise salt dilution (36–38). For the polyglutamate transfer method, histone octamers (0.1 µg/µl) isolated from HeLa cells were incubated with poly-L-glutamate (Sigma, P4886) at a final concentration of 0.2 µg/ml in 10 mM Tris–HCl pH 8.0, 100 mM NaCl overnight at 4°C. This solution was

combined with DNA to achieve histone octamer and DNA concentrations of 50 ng/μl and 25 ng/μl, respectively in 10 mM Tris–HCl pH 8.0, 30 mM NaCl, and then incubated overnight at 37°C. To reconstitute nucleosomal arrays by salt dilution, 1.3 μg of histone octamers were incubated with 1.1 μg of DNA in 20 μl of 2 M NaCl/ HEPES (50 mM HEPES pH 7.5, 1 mM EDTA, 5 mM DTT, 0.5 mM PMSF) for 15 min at 37°C. The reaction was then serially diluted to 1.5, 1, 0.8, 0.7, 0.6, 0.5, 0.4, 0.25 and 0.2 M NaCl by adding the appropriate volume of HEPES buffer followed by incubation for 15 min at 30°C for each step.

For AFM studies, 3 μg of 2-kb SfaNI fragments were used for each reconstitution. The ratio between the DNA and chicken erythrocyte histone octamer was adjusted to 1 or 1.5 (histone/DNA, mass ratio). The histone octamer and DNA were mixed to achieve final concentrations of 0.1 μg/μl DNA and histone octamer, 1× TE (10 mM Tris–HCl pH 7.5, 1 mM $Na_2EDTA$), 1 mM DTT and 1 M NaCl. The mixture was placed on ice for 30 min before stepwise salt dialysis against 0.8 M NaCl, 0.6 M NaCl and 0.15 M NaCl with 1× TE (pH 8.0) buffer for 2 h each at room temperature. The sample was finally dialyzed against 1 mM $Na_2EDTA$ (pH 8.0) overnight at 4°C.

### Micrococcal nuclease digestion

To validate proper reconstitution, an aliquot of 0.5 μg of reconstituted nucleosomal arrays was digested for indicated times (Figure 1B and C) with 12 units of micrococcal nuclease (Worthington) in reaction buffer containing 20 mM Tris–HCl and 2 mM $CaCl_2$ (final concentrations) in a total of 20 μl. Reactions were stopped by 5 mM $Na_2EDTA$. The samples were phenol/chloroform extracted, ethanol precipitated and separated on a 1.5% agarose gel.

To analyze the effect of TRF2 DBD on micrococcal nuclease digestion, nucleosomal arrays were reconstituted on SalI or ScaI digested pRST5, which put the telomeric DNA in the center of the linearized plasmid. Reconstituted nucleosomal arrays (250 ng) with indicated amounts of TRF2 DBD (Figure 4) were digested for 10 min by 6 units of micrococcal nuclease in reaction buffer containing 20 mM Tris–HCl and 2 mM $CaCl_2$ (final concentrations in 20 μl total volume). The reaction was stopped with a mixture of 5 mM $Na_2EDTA$ and 1% SDS, then placed on ice. After digestion with 6 μg proteinase K, the samples were electrophoresed on a 12% native polyacrylamide gel (37.5:1 bis). After staining with SYBR Green (Invitrogen) to observe total DNA present, the gels were transferred to a nylon membrane (Nytran N, Whatman) and detected with a biotin-d(TTAGGG)$_7$ probe using the North2South hybridization and detection kit (Pierce).

### Formation of TRF2 DBD complexes with DNA or nucleosomal arrays

Indicated concentrations of TRF2 DBD were incubated for 30 min at room temperature with 1.73 nM DNA or 2.71 nM reconstituted nucleosomal arrays (166 nM and 260 nM TTAGGG, respectively) in EMSA buffer (20 mM HEPES pH 7.8, 150 mM KCl, 1 mM $MgCl_2$, 20% glycerol). Complexes were either detected by electrophoresis on 0.6% agarose gels in TAE (40 mM Tris–acetate, pH 8.0, 1 mM EDTA) running buffer and staining with SYBR Gold or analyzed by AAGE.

### Analytical agarose gel electrophoresis

Multi-gels were poured using a specially designed apparatus (Aquabogue) and previously described method (24,39). Agarose (Low EEO, Research Organics) concentrations within the multi-gels ranged from 0.25% to 1.0% for data presented in Figure 3A and B, or 0.4–2.0% and 0.7–2.3% for data presented in Figures 3C and D, respectively. Samples were prepared as described for binding experiments. Bromophenol blue/xylene cyanol-loading dye was added to the samples, which were loaded into the multi-gels and run for 3 h at 2 V/cm. One hour before the gel run was finished, charged microspheres (carboxylate, 35 nm radius, Duke Scientific) were added to the gels and samples were electrophoresed for the remaining hour. Gels were stained with SYBR Gold, imaged and migrations were measured with ImageQuant software to obtain electrophoretic mobilities (μ) of DNA/ nucleosomal arrays and microspheres.

Linear portions (0.2–1.3%) of Ferguson plots (semilogarithmic plot of μ versus agarose concentration) were extrapolated to 0% agarose to obtain the gel-free mobility ($\mu'_0$) for DNA, nucleosomal arrays and microspheres. The pore sizes of the gels ($P_e$) for each multi-gel experiment were calculated as described previously (24,39) using the equation,

$$\frac{\mu}{\mu'_0} = \left(1 - \frac{R_e}{P_e}\right)^2 \qquad \qquad \mathbf{1}$$

and $R_e$ of the microspheres (35 nm). To determine the $R_e$ of DNA or nucleosomal arrays, equation [1] was used again, this time with the microsphere-derived $P_e$ values, along with the μ and $\mu'_0$ of DNA or nucleosomal arrays. The $R_e$ values from dilute gels in Figure 3B were obtained by averaging $R_e$ values from 0.25% to 0.6% gels in which no DNA reptation was observed.

### Atomic force microscopy

Histone-free DNA or nucleosomal arrays reconstituted with chicken erythrocyte histones were incubated with TRF2 DBD in EMSA buffer lacking $Mg^{2+}$, at concentrations indicated in Figure 5, for 30 min at room temperature. The resulting complexes were crosslinked with 0.1% glutaradehyde for an additional 30 min and diluted with 1 mM EDTA to 0.3 ng/μl (in DNA) for imaging. A 10 μl aliquot of each sample was deposited on APTES-mica (40), pretreated with 2 μM glutaraldehyde and incubated for 20 min, followed by rinsing with distilled water and drying with nitrogen. The imaging was carried out with a PicoPlus 2500+ [Molecular Imaging, 5500 AFM (N9410S) from Agilent] AFM equipped with a Si3N4 cantilever (AppNano SPM) and a spring constant range from 25 to 75 N/m. The resonance frequency was around 300 kHz; and the scan rate was 1.71 Hz. Gwyddion and

Chromatin Analysis 1.1.7 software was used for image analysis.

### Uptake of single-stranded oligonucleotides by nucleosomal arrays or histone-free DNA

The single-stranded DNA uptake assay was performed similar to the method described previously (31,41). Nucleosomal arrays or histone-free DNA (200 ng), created using undigested or SfaNI digested PRST5, were incubated for 15 min at room temperature, in the presence of TRF2 DBD at specified concentrations, with 100 mM NaCl and reaction buffer containing 50 mM HEPES, 1 mM DTT and 2% glycerol. 5'-$^{32}$P-labeled d(TTAGGG)$_7$ oligonucleotide (T7) was added to a final concentration of 25 nM and the reaction was incubated for an additional 30 min. The reaction was stopped with 1% SDS (final) and 6 μg of proteinase K. Bromophenol blue-loading dye was added and the samples were run on a 1.3% agarose gel in TBE (90 mM Tris–borate, pH 8.3, 2 mM EDTA). The DNA control lane and 1-kb base pair ladder (New England Biolabs) were stained with SYBR Green, while the rest of the gel was dried and then exposed to a phosphorimage screen to detect the presence of the radioactive oligonucleotide.

## RESULTS

In order to analyze the effect of the TRF2 DBDon nucleosomal chromatin fibers, we reconstituted DNA containing 5'-TTAGGG-3' repeats into nucleosomal arrays. TRF2 DBD-dependent changes in the global structure of histone-free DNA and nucleosomal arrays were monitored using atomic force microscopy, micrococcal nuclease digestion and a technique we have termed Analytical Agarose Gel Electrophoresis, AAGE. The AAGE system utilizes a multi-gel apparatus (24,39) to detect changes in macromolecular surface electrical charge density ($\mu_0$), hydrodynamic radius ($R_e$) and 'conformational flexibility' (change in $R_e$ versus gel pore sizes) all in one experiment. The structural analysis of the TRF2 DBD-nucleosomal fibers was correlated to telomere function through a biochemical assay that monitors a reaction associated with t-loop formation and telomere protection.

### Reconstitution of telomeric nucleosomal array fibers

The pRST5 plasmid (17) contains ∼580 bp of telomeric DNA. The plasmid was digested with various enzymes to obtain different substrates for analysis (Figure 1A). To ensure that fragment size and composition did not alter our data interpretation, we analyzed the reconstitution efficiency of both 1-kb and 2-kb telomeric fragments (Figure 1A) into nucleosomal arrays and their binding by the TRF2 DBD (Figure 2). Nucleosomal array fibers were reconstituted with purified histone octamers from HeLa cells using the polyglutamate histone transfer or salt dilution methods (36,38) but higher levels of nucleosome saturation were better achieved with the polyglutamate method. One possible explanation for this is that polyglutamate facilitates assembly on telomeric DNA; previously shown to form relatively less stable nucleosomes

compared to nucleosome-positioning sequences (42,43). Nevertheless, we only used reconstitutes that had a reasonable level of nucleosome saturation in this study. Micrococcal nuclease digestion results (Figure 1B and C) suggest that nucleosomes were properly assembled with periodic spacing. Southern blotting and probing with a telomeric probe (Figure 4B) showed that the 580 bp of telomeric DNA was also assembling into nucleosomes.

AAGE was used to analyze nucleosome saturation levels for each reconstitution. Figure 1D and E illustrate multi-gels of pRST5 digested to obtain 1- and 2-kb telomeric fragments (Figure 1A) either as histone-free DNA or reconstituted nucleosomal fibers. Extrapolation of the Ferguson plot (log μ versus agarose%) to the y-axis provides the gel-free mobility or $\mu_0'$, which is proportional to the electrical surface charge density of the macromolecule (24,39). Since this term refers to a density of charges, it was expected that similar values would be achieved for the different DNA fragments, and this is demonstrated by the results for the 208-12 and telomeric DNA in Supplementary Table I. The histone octamer contributes positive charge to the fiber surface through its lysine/arginine-rich tail domains. In addition, a smaller amount of negative surface charge neutralization is contributed by a positively charged surface created by the histone-fold domains that interact with DNA assembled in the nucleosome core (44,45). Consequently, properly assembled nucleosomes should result in a defined level of DNA negative surface charge neutralization that is proportional to the number of nucleosomes per DNA base pair (24). Analysis of the effect of nucleosomal saturation on the $\mu_0'$ of nucleosomal arrays in low salt buffers has been extensively characterized with the 208-12 DNA template, which contains 12 repeats of the Sea Urchin 5S nucleosome positioning DNA (32,46). The $\mu_0'$ term was highly reproducible, and a linear drop in negative surface charge density with increasing nucleosome assembly correlated well with an increase in $s_{20,w}$ (24), with an ∼20% drop in negative charge pertaining to ∼1 nucleosome/208 bp of DNA. As shown in Supplementary Table I, a ∼22–25% drop in $\mu_0'$ was observed for the telomeric DNA fragments as they were saturated with nucleosomes.

Nucleosome saturation is also revealed by a drop in the effective radius ($R_e$) (24). In order to calculate the effective radii ($R_e$) of the DNA and chromatin, the pore sizes ($P_e$) of the gels must be obtained. Previously, bacteriophage T3, a spherical bacteriophage with a 30.1 nm radius, was added to samples to calculate the $P_e$ for each gel concentration (24). We tested whether similar multi-gel pore sizes could be attained with commercially available, carboxylate-coated microspheres. Figure 1F shows that $P_e$ values derived from multi-gel experiments with microspheres were similar to those achieved with bacteriophage T3.

The $R_e$ of both DNA and nucleosomal arrays remains constant in dilute gels (averaged from 0.25–0.6% gels) and is likely a reflection of the hydrodynamic radius of the molecules in solution. This is demonstrated by a decrease in $R_e$ with increasing nucleosome saturation on the 208-12 DNA template, which coincided with an increase in $s_{20,w}$ (24). The $R_e$ in dilute gels of the 208-12 and 2-kb telomeric fragments were reduced by 40–50% with nucleosome
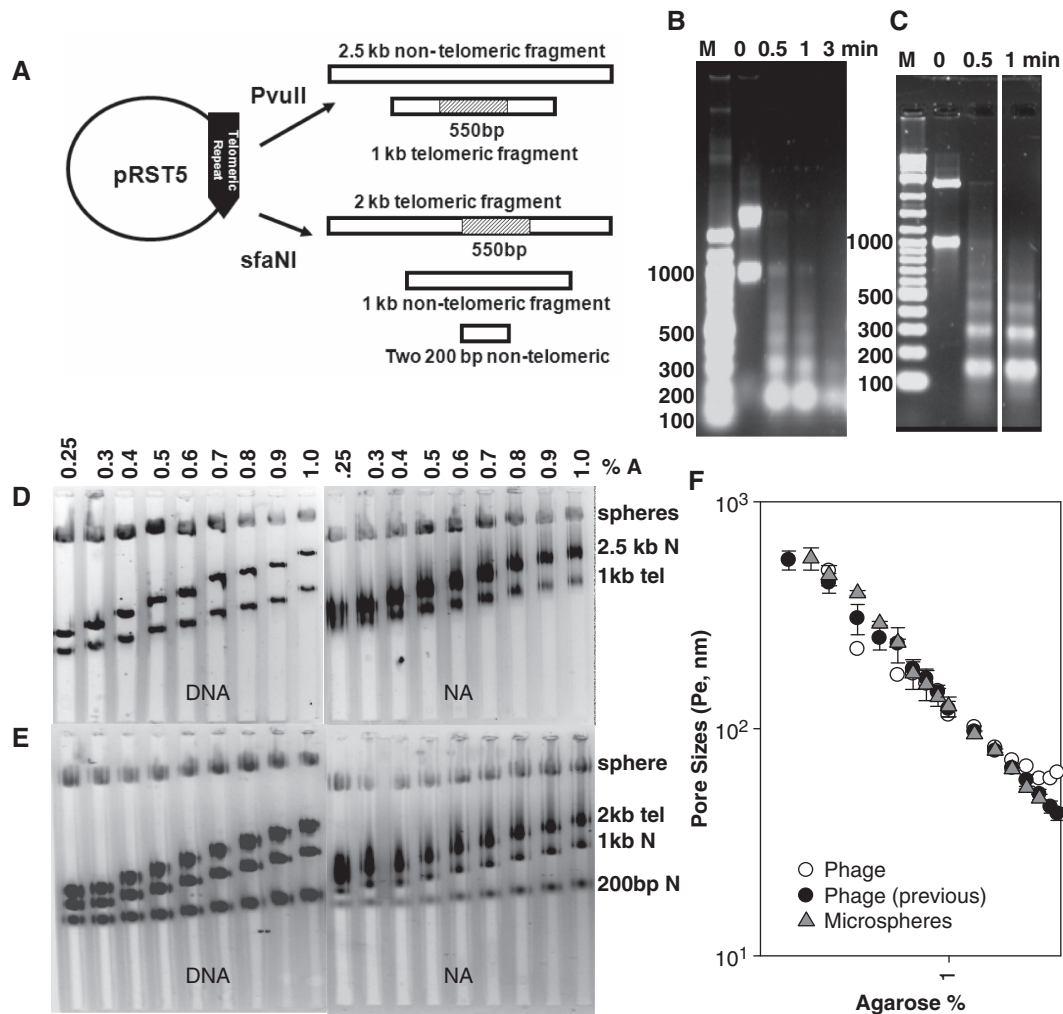
**Figure 1.** Analysis of nucleosomal array fibers. The pRST5 plasmid and expected fragments created by PvuII or SfaNI digestion (**A**). Micrococcal nuclease digestion at indicated time points of nucleosomal arrays reconstituted onto PvuII (**B**); SfaNI (**C**) digested pRST5 DNA. Multi-gels of telomeric nucleosomal array fibers (NA) and histone-free DNA (DNA) from pRST5 digested with PvuII (**D**); and SfaNI (**E**) prepared and subjected to electrophoresis according to 'Materials and Methods' section. Spheres refer to carboxylate-coated microsphere standards (35 nm radius). The '1 kb tel' and '2 kb tel' refer to the telomeric fragments liberated by PvuII and SfaNI digestion respectively. 'N' refers to the fragments without telomeric DNA. Logarithmic plot of pore sizes ($P_e$) versus agarose% (**F**). Data was obtained from multi-gels run with bacteriophage T3 (Phage) in this laboratory or previous work [Phage, previous, (24)] and 35 nm carboxylate-coated microspheres (Microspheres). $P_e$ for each agarose concentration was calculated according to 'Materials and Methods'. Symbols with error bars represent the mean ± 1 SD of four to eight determinations.

reconstitution (Supplementary Table I). The $R_e$ of the 1-kb telomeric DNA was only reduced by ~20%, which is similar to that observed with reconstitution of 208-5 DNA (T. M. Fletcher and J. C. Hansen, unpublished results). From the $\mu_0'$ and $R_e$ data we can infer that the nucleosomal arrays had a density of ~1 nucleosome per 170–190 bp or 11–12 nucleosomes on the 2-kb fragment and only reconstituted material with this level of saturation was used in experiments.

The nucleosome density of the reconstitutes was also determined by atomic force microscopy. Nucleosomal array fibers reconstituted with the 2-kb telomeric fragment using a 1-1.5:1 mass ratio of histone octamer to DNA typically had an average of 12 nucleosomes (Supplementary Figure 1A and C) indicating a level of saturation in agreement with the AAGE analysis. To ensure that proper nucleosomes were assembled, heights of the nucleosomal

structures within the fibers were determined. The maximum height distributions ranged from 2.5 to 3.5 nm (Supplementary Figure 1B and D), in agreement with previous findings (47).

## The TRF2 DBD interacts specifically with telomeric DNA and nucleosomal arrays

Binding of TRF2 DBD to the 1-kb and 2-kb fragments containing 580 bp of telomeric DNA (~95 TRF2 DBD-binding sites) was detected by a decrease in mobility in 0.6% agarose gels (Figures 2A and C, telo). As expected, the mobility of non-telomeric DNA (N-telo) was not affected by TRF2 DBD. This demonstrates that the TRF2 DBD bound specifically to telomeric DNA. Interestingly, the mobility of nucleosomal arrays was shifted more by lower concentrations TRF2 DBD than that of histone-free DNA. However, the nucleosomal
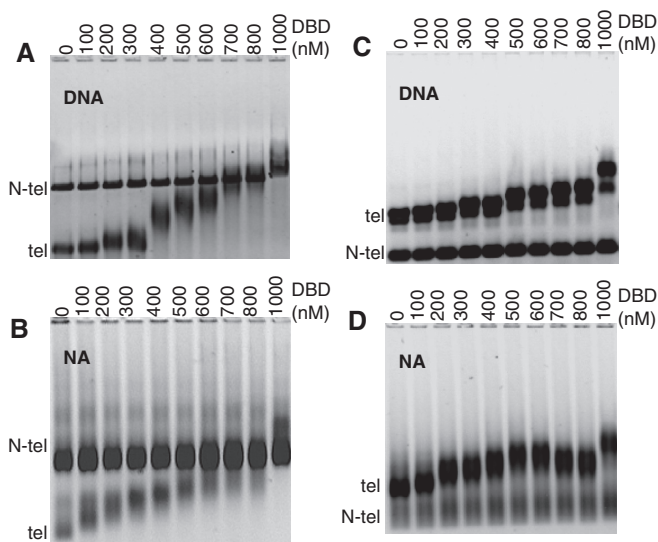
**Figure 2.** TRF2 DBD binds specifically to telomeric DNA and nucleosomal arrays. 0.6% agarose gels of TRF2 DBD binding to DNA (DNA) (**A**) and nucleosomal arrays (NA) (**B**) from the pRST5 fragment digested to obtain a 1-kb DNA fragment with 580-bp telomeric DNA (telo) and 2.5-kb non-telomeric DNA (N-telo). Gels similar to (A) and (B), respectively except the pRST5 was digested to obtain a 2-kb fragment containing the 580-bp telomeric DNA (telo) with a 1 kb and smaller fragments being non-telomeric (N-telo) (**C** and **D**).

array mobility shift leveled off at higher TRF2 DBD concentrations. It is possible that the mobility of nucleosomal arrays leveled off at the higher concentrations because the binding sites became saturated. The apparent Kd of TRF2 DBD with a 5′-GTTAGGGTTAGGG-3′ oligonucleotide ranged from 180 to 750 nM depending on the KCl concentration (48). It is important to note that the concentration of TRF2 DBD-binding elements in our studies is likely to be near the Kd of TRF2 DBD since the fragments contain ~96 TTAGGG repeats.

The TRF2 DBD-induced mobility shifts are likely due to changes in charge, size and shape of the DNA and nucleosomal fibers which can be assessed by AAGE. To ensure that the TRF2 DBD-DNA and TRF2 DBD-nucleosomal array complexes were stable during AAGE experiments, the samples were electrophoresed at a higher voltage potential in two dimensions (Supplementary Figures 2A and B). If electrophoresis causes the complexes to dissociate, the samples should have a higher apparent migration rate in the second dimension. However, the complexes appear to have a similar mobility in the second dimension as the first, suggesting that they are stable enough to be studied with AAGE.

Another potential complication is that mobility shifts may be caused by interactions of these complexes with the gel fibers, which may slow down the migration rate resulting in misleading data. If interactions with the gel matrix significantly reduced the migration rate, higher concentrations of both TRF2 DBD and either DNA or nucleosomal arrays should result in faster migration rates since some of the sample will 'coat' the gel fibers, allowing the rest of the sample to proceed. Supplementary Figure 2C and D show that a nearly 10-fold increase in

TRF2 DBD-DNA or TRF2 DBD-nucleosomal array fiber concentration resulted in even slower migration rates, suggesting that the mobility shifts are mainly due to changes in complex charge and structure as opposed to interactions with the gel. Also, note that the highest concentrations of both TRF2 DBD and DNA or nucleosomal arrays resulted in a mobility shift of the non-telomeric DNA, suggesting that some binding specificity was lost, but at concentrations significantly higher than the AAGE experiments in this study. Both of these controls demonstrate that the observed mobility shifts are most likely due to TRF2 DBD-dependent changes in surface charge density and effective radius, which can be revealed by AAGE analysis.

### The TRF2 DBD reduces negative surface charge density on nucleosomal fibers more than histone-free DNA

AAGE was used to determine the differential effects of the TRF2 DBD on the biophysical characteristics of nucleosomes and histone-free DNA. Since the TRF2 DBD is a relatively basic DNA-binding domain, it was expected to neutralize some of the DNA charge when bound. Indeed, increasing concentrations of the TRF2 DBD (Figure 3A) resulted in a drop in DNA surface charge density ($\mu_0'$) until ~20% less negative surface charge was observed at 1 μM TRF2 DBD (a mole ratio of ~6 TRF2 DBD: 1 TTA GGG). If the $\mu_0'$ accurately represents changes in the charge density as TRF2 DBD fills TTAGGG sites, the TRF2 DBD should have a greater effect on the $\mu_0'$ of the 1-kb fragment. The 1-kb fragment has twice the density of TRF2 DBD-binding sites than the 2-kb fragment. This was indeed the case (Figure 3A). Interestingly, the TRF2 DBD also caused a more dramatic drop in negative surface charge of the 2-kb nucleosomal arrays than the 2-kb histone-free DNA (Figure 3A), suggesting that TRF2 DBD has unique binding interactions with telomeric nucleosomal arrays and/or it alters their structure.

### The TRF2 DBD increases the effective radius of nucleosomal arrays but not that of histone-free DNA

The TRF2 DBD may be neutralizing more negative surface charge on the nucleosomal array because it is inducing a conformational change when it binds to the fiber. A TRF2 DBD-induced conformational change was detected with AAGE by observing a TRF2 DBD-dependent change in $R_e$. The radii from dilute gels (0.25–0.6%), where the gel fibers were least likely to affect macromolecular structure, were averaged for each multi-gel experiment. Comparison of changes in sedimentation coefficient and the $R_e$ in dilute gels with nucleosome assembly levels, $Mg^{2+}$-dependent nucleosomal array folding, or reconstitution of sub-nucleosomal arrays demonstrate that this parameter can reflect a hydrodynamic radius similar to a Stokes radius (24,26–28).

Binding of the TRF2 DBD to histone-free DNA resulted in only a slight increase in $R_e$ (Figure 3B). However, binding of the TRF2 DBD at low concentrations to nucleosomal arrays gradually increased their $R_e$ until they were ~40% larger than the control (Figure 3B). This effect appeared to level off (or even partially reversed)
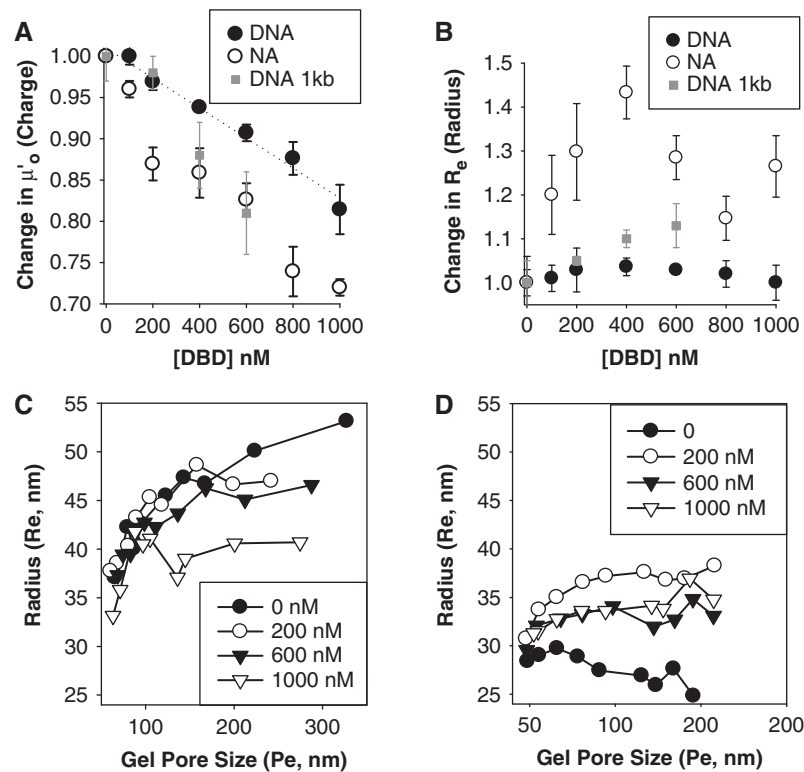
**Figure 3.** TRF2 DBD-dependent changes in surface charge density ($\mu'_0$), effective radius ($R_e$ from dilute gels) and conformation flexibility ($R_e$ versus $P_e$). The $\mu'_0$ at each indicated TRF2 DBD concentration was obtained by Ferguson plots of mobilities derived from multi-gels with agarose concentrations of 0.25–1% according to 'Materials and Methods' section (**A**). The $R_e$ at each TRF2 DBD concentration derived from 0.25–1% multi-gel experiments according to 'Materials and Methods' section (**B**). The $R_e$ values from 0.25–0.6% agarose (dilute gels) were averaged from each multi-gel experiment. The $\mu'_0$ or $R_e$ for each TRF2 DBD concentration was normalized to 0 nM TRF2 DBD. Each data point represents the mean ± 1 SD of 3-7 multi-gel experiments. The effect of the TRF2 DBD on the reptation of DNA and nucleosomal arrays (change in $R_e$ versus $P_e$) in concentrated gels (**C** and **D**). Plots of effective radius ($R_e$) versus pore size ($P_e$) of DNA (**C**) or nucleosomal arrays (**D**) incubated with indicated amounts of TRF2 DBD. $R_e$ and $P_e$ were derived from multi-gels of 0.7–2.5% agarose concentrations or 0.4–2.1% agarose concentrations according to 'Materials and Methods' section. The DNA fragment analyzed in all experiments in this figure was the 2-kb telomeric fragment unless otherwise indicated.

with further addition of TRF2 DBD (Figure 3B, >400 nM TRF2 DBD).

The $\mu_o$ and $R_e$ data in Figure 3 are consistent with the binding data in Figure 2 where increasing levels of TRF2 DBD resulted in a more gradual shift in mobility of telomeric histone-free DNA in a single concentration agarose gel. Since very little change in the $R_e$ of telomeric DNA was observed, this gradual change in mobility can be largely attributed to the apparent linear decrease in negative surface charge density. However, the mobility of nucleosomal arrays was shifted more by TRF2 DBD at lower concentrations, which then leveled off at higher TRF2 DBD concentrations. These TRF2 DBD-dependent effects on the mobility of nucleosomal arrays can be attributed to both a greater reduction of negative surface charge density relative to histone-free DNA, and an increase in radius. In addition, the leveling off of the mobility at higher TRF2-DBD concentrations corresponds to a lack of increase in $R_e$ with increasing TRF2 DBD.

**The TRF2 DBD alters the ability of telomeric DNA and nucleosomal array fibers to reptate through the gel pores**

Although DNA is thought to exist as a random coil in solution, with a predicted average radius based on the

length of the DNA chain and its persistence length, its movement has been shown to be restricted by the gel matrix. The outcome is that DNA reptates through the gel by both stretching and end-first movement through the pores (49–51). This suggests that DNA has a degree of conformational flexibility that depends mainly on its persistence length. Reptation can be observed in 2-D gels by increased mobility of DNA at higher voltage potentials relative to spherical bacteriophage standards (24). Reptation of DNA can also be observed with the AAGE technique when samples are electrophoresed in multi-gels with high concentrations of agarose where the gel pores impinge upon the structure of the DNA (24). Reptation is demonstrated by a decrease in $R_e$ as a function of decreasing pore sizes ($P_e$). As expected, DNA, in the absence of TRF2 DBD, reptated in more concentrated gels (Figure 3C). Although reptation was only slightly affected by adding 200 and 600 nM TRF2 DBD, it was significantly reduced in the presence of 1000 nM TRF2 DBD, suggesting that extensive binding of the TRF2 DBD to the tandem binding sites reduced the conformational flexibility of the DNA.

Assembly of the 208-12 DNA into an array of nucleosomes results in a structure that does not appear to be

altered by decreasing gel pore size. Instead, reducing the gel pore sizes causes the nucleosomal arrays to move slower through the gel matrix (24). The likely explanation for this is that, depending on the internucleosomal spacing, the linker DNA is shorter than the persistence length resulting in a nucleosomal fiber that is relatively less flexible. As expected, the $R_e$ of telomeric nucleosomal arrays, in the absence of TRF2 DBD, was unaltered by a decrease in $P_e$ (Figure 3D). The presence of 200 nM TRF2 DBD resulted in a structure with a larger $R_e$ in more dilute gels where $P_e > 100$ nm (Figure 3B and D). However, a gradual decrease in $R_e$ was observed for this structure as gel pores were reduced below 100 nm (Figure 3D), indicating that low concentrations of TRF2 DBD increased the conformational flexibility of nucleosomal fibers allowing them to reptate through the gel pores. However, the nucleosomal fibers in the presence of 600 and 1000 nM TRF2 DBD (Figure 3D) did not substantially reptate, even though the complexes formed at these TRF2 DBD concentrations were larger than nucleosomal array fibers in the absence of TRF2 DBD. This suggests that the flexibility initiated by low-level binding of TRF2 DBD binding was lost as additional TRF2 DBD loaded onto the nucleosomal arrays.

## TRF2 DBD protects nucleosomal arrays from micrococcal nuclease digestion

The increase in $R_e$ and flexibility of nucleosomal fibers in the presence of low concentrations of TRF2 DBD suggests some form of nucleosome disruption or nucleosome sliding. Both of these scenarios should be detected by alterations in micrococcal nuclease digestion. To observe nucleosome disruption, nucleosomal fibers were subjected to micrococcal nuclease digestion under conditions that yield mostly mononucleosome with some di- and trinucleosomal fragments as detected on native polyacrylamide gels (Figure 4). Staining gels with SYBR Green showed that nucleosome cores remained largely intact throughout the nucleosomal fiber in the presence of low concentrations of TRF2 DBD (Figure 4A). A Southern blot with a telomeric DNA probe confirmed that telomeric nucleosomes remained intact with TRF2 DBD concentrations up to 500 nM (Figure 4B). If the increase in flexibility observed in Figure 3D was due to TRF2 DBD-induced nucleosome sliding, a smearing of the mono-, di- and trinucleosomal bands would be apparent; however, this did not appear to be the case. These results suggest that the increase in radius and flexibility observed in Figure 3 were not due to significant nucleosome disruption or sliding. The AAGE and mobility shift data in Figures 2 and 3 show that TRF2 DBD has different effects on nucleosomal arrays at higher concentrations. This coincided with the weak appearance of an ~600-bp micrococcal nuclease resistant fragment in the SYBR Green-stained gels (Figure 4A), which was slightly larger than the trinucleosomal fragment. The telomeric DNA-specific Southern blot revealed that this band pertained to telomeric DNA that became significantly inaccessible to micrococcal nuclease (Figure 4B).
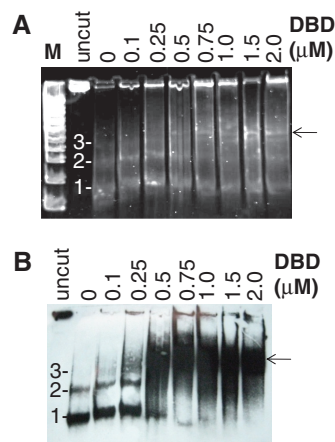


**Figure 4.** TRF2 DBD-dependent changes in micrococcal nuclease digestion. Nucleosomal arrays (12.5 ng/ul) were incubated with indicated amounts of TRF2 DBD and digested with micrococcal nuclease according to 'Materials and Methods' section. Deproteinated samples were electrophoresed on a 12% native polyacrylamide gel and stained with SYBR Green (**A**) followed by transfer to a membrane and blotting with a biotin-d(TTAGGG)$_7$ probe (**B**) as described in the 'Material and methods' section. M refers to 100-bp ladder. The 1-, 2-, 3- to the left of the gel *panels* refer to mono-, di- and trinucleosomes, respectively.

## AFM of TRF2 DBD complexed with DNA and nucleosomal array fibers

The AAGE data in Figure 3 demonstrated that addition of TRF2 DBD did not increase the $R_e$ beyond a concentration of 400 nM even though the negative charge continued to decrease as the concentration was raised to 1000 nM. Moreover, access of micrococcal nuclease to the fibers was dramatically reduced at TRF2 DBD concentrations of >500 nM. These results suggest that the TRF2 DBD continued to bind beyond 400 nM concentrations but may have induced compaction. To analyze further the effect of the TRF2 DBD on the structure of nucleosomal arrays, single molecules were visualized by AFM. Here TRF2 DBD was first incubated with telomeric nucleosomal arrays then fixed with glutaraldehyde and adhered to AP-mica slides. AFM images were obtained of nucleosomal array fibers in the presence of 0–1000 nM TRF2 DBD.

Observation of individual fibers in the presence of TRF2 DBD revealed larger complexes frequently located in the center of the fiber, suggesting that TRF2 DBD is preferentially binding to telomeric sequence (Supplementary Figure 3C and E). Interpreting this data alone, it is not clear whether TRF2 DBD is binding specifically to nucleosomes, displacing a nucleosome or inducing compaction. However, the micrococcal nuclease digestion results were not consistent with nucleosome displacement (Figure 4), and an increase in $R_e$ (Figure 3B) at low TRF2 DBD concentrations was not consistent with significant compaction. Complexes were also observed on histone-free DNA (Supplementary Figure 3F).

Quantifying TRF2 DBD-dependent changes in the structure of nucleosomal fibers was achieved by analysis of fiber heights and contour length as a function of TRF2 DBD concentration (Figure 5 and Supplementary
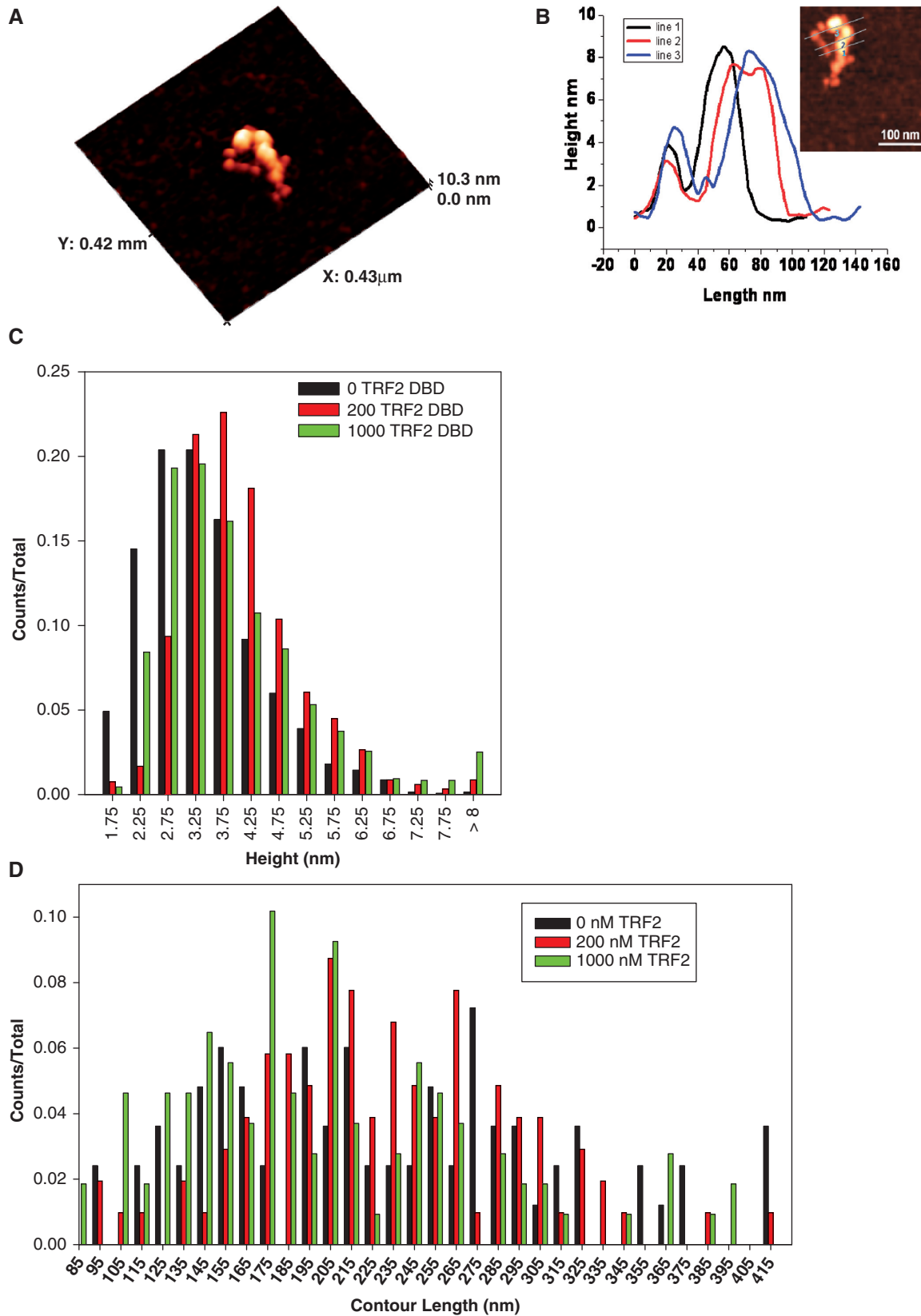
**Figure 5.** Atomic force microscopy of TRF2 DBD-nucleosomal array complexes. A nucleosomal array fiber in the presence of 200 nM TRF2 DBD with a scale of the plane in the *X* and *Y* directions (0.43 and 0.43 μm, respectively) and height scale from 0 to 10 nm (**A**). Example of a height versus length plot of the complex in (A) obtained by Gwyddion software (**B**). Comparison of TRF2 DBD-dependent fiber height distributions by normalizing counts of fibers (Supplementary Figure 4) having indicated heights to total number of fibers (**C**). Comparison of TRF2 DBD-dependent fiber contour length distributions by normalizing counts of fibers (Supplementary Figure 5) having indicated contour lengths to total number of fibers (**D**). Contour lengths were generated with Chromatin Analysis 1.1.7 software.
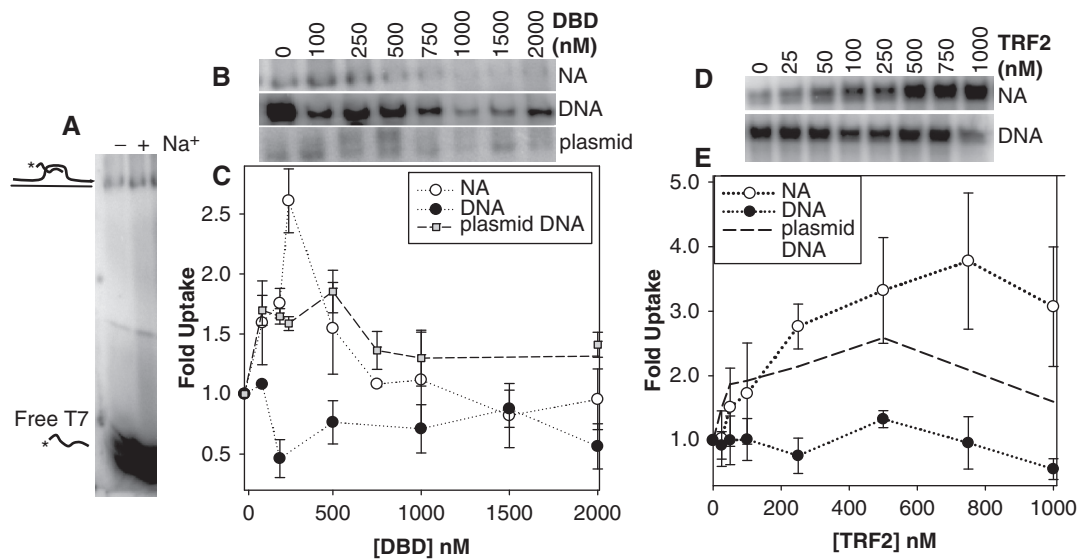
**Figure 6.** The effect of full-length TRF2 and TRF2 DBD on the uptake of a 5′-[$^{32}$P]-labeled, single-stranded oligonucleotide, (dTTAGGG)$_7$ (T7), into nucleosomal arrays and DNA (20 ng/μl). Samples were incubated with indicated amounts of full-length TRF2 or TRF2 DBD and processed according to 'Materials and Methods'. Uptake by nucleosomal arrays with samples incubated – or + 100 mM NaCl (**A**). The drawings on the side of the agarose gel refer to radiolabeled (∗) T7 oligonucleotide either free or inserted into the nucleosomal arrays. A section of agarose gels showing T7 inserted into nucleosomal arrays (*top panel*), linear DNA (*middle panel*) and plasmid DNA (*bottom panel*) with increasing TRF2 DBD (**B**). Quantitation of (B) where uptake was normalized to 0 nM TRF2 DBD (**C**). Error bars are 1 SD of the mean of 3–5 determinations. Full-length TRF2-dependent uptake by nucleosomal arrays (*top panel*), linear DNA (*bottom panel*) (**D**). Quantitation of (D) where uptake was normalized to 0 nM TRF2 (**E**). The dashed line refers to uptake by supercoiled pRST5 from previous work (41). Error bars are 1 SD of the mean of three to four determinations.

Figures 4 and 5). Nucleosomes typically have heights that vary from 2.5 to 3.0 nm (Supplementary Figure 1D). Figures 5A and B illustrate an example of a nucleosomal fiber in the presence of TRF2 DBD that has structures with heights in the nucleosomal (∼3 nm), intermediate-sized (4–6 nm) and taller (>6 nm) ranges. Histograms of the number of molecules (counts) with observed heights were generated for each TRF2 DBD concentration (Supplementary Figure 4). These were then normalized to total counts to allow for direct comparison between TRF2 DBD concentrations (Figure 5C). The presence of 200 nM TRF2 DBD shifted the population of fiber heights from around 3 nm to closer to 4 nm. In addition, there was an increase in the population of fibers with heights ranging from 4 to 8 nm. Increasing the concentration of TRF2 DBD from 400 to 1000 nm did not increase the number of fibers with intermediate heights, but increased the number of fibers with heights >6 nm.

An increase in heights could be due to TRF2 DBD–nucleosome complexes, fiber compaction, or both. To determine whether fibers compact, contour lengths were measured as a function of TRF2 DBD concentration (Figure 5D and Supplementary Figure 5). In the absence of TRF2 DBD, a broad distribution of fiber lengths was observed that centered around 240 nm. Addition of 200 nM TRF2 DBD resulted in a more narrow length distribution, but it was still centered at 240 nm. This was also observed in the presence of 400 nM TRF2 DBD (Supplementary Figure 5). However, further addition TRF2 DBD (1000 and 2000 nM) significantly increased the population of fibers with contour lengths <200 nm,

suggesting that TRF2 DBD concentrations of >400 nM induced fiber compaction.

### The TRF2 DBD increases uptake of a single-stranded telomeric oligonucleotide by nucleosomal arrays

One of the major functions of TRF2 is the protection of chromosome ends. TRF2 is thought to perform this function by stabilizing a t-loop structure, which safeguards the 3′ G-strand overhang from undesirable DNA metabolism and damage signaling (16). The structure involves looping back of the telomere end allowing for invasion of the terminal 3′ overhang into the duplex region and creating a displacement or D-loop (16). Telomeric D-loop formation has been mimicked by observing the uptake of a labeled single-stranded telomeric oligonucleotide by a double-stranded plasmid containing telomeric DNA, in the presence of crude cellular extracts or recombinant TRF2 (31,41,52). Uptake only occurs with telomeric DNA sequence and the process is stimulated by the addition of Na$^+$ and TRF2 (31,41). TRF2 was shown to alter DNA topology through a dimerization domain (TRFH), destabilizing the plasmid duplex DNA and providing an opportunity for annealing of the telomeric oligonucleotide (31).

Since the most likely substrate for TRF2 binding and t-loop formation at the telomeres is nucleosomal chromatin, we chose to analyze the effects of full-length TRF2 and the TRF2 DBD on the insertion of a $^{32}$P-labeled, d(TTAGGG)$_7$, single-stranded oligonucleotide (T7) into reconstituted telomeric nucleosomal fibers (Figure 6A). The results with nucleosomal arrays were compared

with histone-free linear and supercoiled plasmid DNA. The presence of 100 mM $Na^+$ stimulated the insertion of labeled T7 into unlabeled, nucleosomal fibers (Figure 6A), similar to that observed with histone-free supercoiled plasmid DNA (41). A further stimulation of this reaction was observed with increasing TRF2 DBD up to 500 nM, at which point the stimulation was lost; further addition of TRF2 DBD inhibited the reaction (Figure 6B and C). Note that the loss in stimulation at 500 nM TRF2 DBD coincided with a change in the effect of TRF2 DBD on the $R_e$, flexibility and access of micrococcal nuclease (Figures 3 and 4). The TRF2 DBD-dependent stimulation of T7 uptake was not observed with histone-free, linear DNA (Figure 6B and C). Interestingly, the TRF2 DBD also promoted T7 uptake by supercoiled plasmid DNA but this effect was not as dramatic as that observed with nucleosomal fibers. Moreover, higher concentrations TRF2 DBD did not inhibit the reaction with supercoiled plasmid DNA as much as was observed with nucleosomal fibers.

Similar to the effect with TRF2 DBD, full-length TRF2 increased T7 uptake by nucleosomal fibers (Figure 6D and E). In contrast to that observed with TRF2 DBD, additional TRF2 stimulated the reaction even further, up to a nearly 4-fold increase with 800 nM TRF2. A TRF2-dependent increase in oligonucleotide uptake by supercoiled, histone-free DNA was also observed [Figure 6D and E and (31,41)] but to a lesser extent than the uptake by nucleosomal fibers. As with TRF2 DBD, TRF2 did not substantially increase T7 uptake by linear DNA. Together these results suggest that both TRF2 and TRF2 DBD stimulated reactions of T7 with nucleosomal arrays and supercoiled plasmids more than linear DNA. Moreover, TRF2 DBD-dependent effects on the reaction with nucleosomal arrays paralleled the effects on nucleosomal array structure. Finally, full-length TRF2 not only was more efficient at stimulating this reaction, but also did not inhibit the reaction at higher concentrations, suggesting that optimal formation of t-loops in the context of nucleosomal arrays requires more than just the DBD.

## DISCUSSION

This work represents the first biophysical analysis of the interactions of a myb/SANT DBD with its sites within nucleosomal array fibers. Nucleosomal arrays with telomeric DNA sequence were successfully reconstituted *in vitro* with an acceptable level of nucleosome saturation and spacing similar to that observed *in vivo*. The TRF2 DBD bound to telomeric DNA and nucleosomal arrays with little non-specific binding to non-telomeric DNA sequence.

Analytical agarose gel electrophoresis has been a useful tool in characterizing solution attributes of nucleosomal array fibers (24,27,28,39). This study extends the work on nucleosomal array fibers to observe how a DNA-binding factor alters their overall structure. As shown in earlier studies, the surface charge density parameter has been surprisingly informative in providing explanations for changes in chromatin structure. In this study, we found that TRF2 DBD reduced more negative surface charge density on the 2-kb nucleosomal fibers than histone-free DNA. One explanation for this is that TRF2 DBD has a higher affinity for the DNA within nucleosomal arrays than histone-free DNA. However, binding studies with the homologous TRF1 and telomeric mononucleosomes show that assembling telomeric DNA into nucleosomes significantly reduces the affinity of TRF1, particularly when its binding elements are near the nucleosome dyad and facing toward the histones (23). In fact, yeast Rap1p also has a lower affinity for mononucleosomes when the binding sites are near the dyad and its myb/SANT DBD has an even lower affinity for nucleosomal DNA even when its element is placed near the nucleosome edge (22). Another explanation is that the TRF2 DBD may have a higher affinity for nucleosomal fibers by interacting with histone tails similar to other myb/SANT domains (53–56).

The TRF2 DBD may also reduce the negative charge on nucleosomal arrays by inducing a conformational change. Earlier studies with AAGE demonstrated that $Mg^{2+}$-dependent fiber compaction was associated with a decrease in both $\mu_o$ and $R_e$ (26). The loss of negative charge from the surface was attributed to the loss of DNA (and associated counterions) from the surface of the compacted fiber. The study here shows that TRF2 DBD had two effects on the structure of nucleosomal fibers, depending on the amount of TRF2 DBD added to the mixture. The results at higher concentrations are partially consistent with fiber compaction. While the surface charge density continued to decrease with increasing TRF2 DBD concentrations, the $R_e$ only increased with TRF2 DBD concentrations up to 400 nM at which point it leveled off or even decreased. This could be due to a saturation of binding sites. However, the surface charge density continues to decrease with increasing TRF2 DBD concentrations and there is no evidence of binding to the non-telomeric fiber, suggesting that the TRF2 DBD continues to bind to telomeric DNA within the fiber (Figure 2). AFM images showed that TRF2 DBD formed large complexes along the nucleosomal fiber with increased heights, while higher TRF2 DBD concentrations reduced the contour length. The reduction in negative surface charge density, $R_e$, flexibility, contour lengths and micrococcal nuclease digestion of the telomeric region are consistent with TRF2 DBD filling TTAGGG sites within the fiber and inducing some type of compaction. It should be noted that the level of fiber compaction in this study is less than that observed with AAGE in the presence of $Mg^{2+}$ (26) or linker histones (29) partly because it is restricted to the telomeric region of the fiber. Furthermore, the striking lack of access of micrococcal nuclease to the telomeric DNA suggests that the three nucleosomes in that region form a unique higher-order structure as illustrated in the AFM image in Figure 5.

The mechanism and precise nature of the conformational changes occurring with lower concentrations of TRF2 DBD is more complicated. TRF2 DBD binding increased both the radius and flexibility of the

nucleosomal fiber (Figure 3B and D). This is consistent with some kind of 'loosening' of the fiber structure but it is unclear whether this type of conformational change should reduce the negative charge on the surface of the fiber. TRF2 DBD could also be interacting with linker DNA and extending the structure. However, a significant reduction of micrococcal nuclease access to linker DNA was only observed with higher concentrations of TRF2 DBD (Figure 4). Alternatively, TRF2 DBD may promote the intrinsic ability of telomeric nucleosomes to slide to a new position (57). This should result in TRF2 DBD-dependent smearing of the nucleosome repeat ladder with micrococcal nuclease digestion, yet little smearing was observed (Figure 4). Another alternative is that TRF2 DBD disrupts nucleosome structure. Interestingly, overexpression of full-length TRF2 in epithelial cells disrupts telomeric chromatin associated with histone loss (58). Our results may be consistent with this, since earlier studies with AAGE showed that a reduction of nucleosome density, removal of H2A/H2B dimers or histone 'tail' domains increased the size and flexibility of nucleosomal fibers (24,26–28). However, the lack of subnucleosomal fragments in the micrococcal nucleosome digest (Figure 4) suggests that telomeric nucleosomes were still largely intact in the presence of TRF2 DBD. Perhaps the alteration in nucleosome structure by TRF2 DBD is more subtle. The homologous TRF1 did not eject histones from mononucleosomes *in vitro* but DNase I hypersensitive sites were observed in TRF1-mononucleosome complexes implicating an alteration in nucleosome structure (23).

We propose that the effect of TRF2 DBD on nucleosomal array structure is at least partly responsible for the observed increase in the access of a single-stranded d(TTA GGG)$_7$ oligonucleotide (Figure 6). This would be an interesting finding since telomeric chromatin is nucleosomal, and would suggest an additional role of TRF2 in promoting t-loops: modulation of the chromatin structure. It has been shown that TRF2 can change DNA topology but through the TRFH domain, thereby weakening the duplex DNA within a supercoiled plasmid and allowing for annealing of the free oligonucleotide (31). In cells, this reaction is proposed to occur between the duplex region of the telomere and the G-strand overhang (16). We now show that by distorting the structure of the fiber and/or nucleosomes, the DNA-binding domain of TRF2 may also be involved in promoting this reaction. Interestingly, high concentrations of TRF2 DBD inhibited the uptake of the single-stranded oligonucleotide by nucleosomal arrays (Figure 6), suggesting that either loading of telomeric DNA with TRF2 DBD and/or fiber compaction has the ability to inhibit a strand invasion-like reaction. This inhibition was not observed with full-length TRF2. Most importantly, the described structural and biochemical effects of TRF2 DBD on nucleosomal arrays were not observed with histone-free DNA. The differential effects of TRF2 DBD on telomeric nucleosomal arrays, as opposed to histone-free DNA, emphasize the importance of analyzing the interactions of DNA-binding factors with a more native substrate such as nucleosomal chromatin.

## REFERENCES

1. Luger,K., Mader,A.W., Richmond,R.K., Sargent,D.F. and Richmond,T.J. (1997) Crystal structure of the nucleosome core particle at 2.8 Å resolution. *Nature*, **389**, 251–260.
2. McBryant,S.J., Adams,V.H. and Hansen,J.C. (2006) Chromatin architectural proteins. *Chromosome Res.*, **14**, 39–51.
3. McCord,R.A. and Broccoli,D. (2008) Telomeric chromatin: roles in aging, cancer and hereditary disease. *Mutat. Res.*, **647**, 86–93.
4. Bedoyan,J.K., Lejnine,S., Makarov,V.L. and Langmore,J.P. (1996) Condensation of rat telomere-specific nucleosomal arrays containing unusually short DNA repeats and histone H1. *J. Biol. Chem.*, **271**, 18485–18493.
5. Makarov,V.L., Lejnine,S., Bedoyan,J. and Langmore,J.P. (1993) Nucleosomal organization of telomere-specific chromatin in rat. *Cell*, **73**, 775–787.
6. Wu,P. and de Lange,T. (2008) No overt nucleosome eviction at deprotected telomeres. *Mol. Cell Biol.*, **28**, 5724–5735.
7. Murga,M., Jaco,I., Fan,Y., Soria,R., Martinez-Pastor,B., Cuadrado,M., Yang,S.M., Blasco,M.A., Skoultchi,A.I. and Fernandez-Capetillo,O. (2007) Global chromatin compaction limits the strength of the DNA damage response. *J. Cell Biol.*, **178**, 1101–1108.
8. Garcia-Cao,M., O'Sullivan,R., Peters,A.H., Jenuwein,T. and Blasco,M.A. (2004) Epigenetic regulation of telomere length in mammalian cells by the Suv39h1 and Suv39h2 histone methyltransferases. *Nat. Genet.*, **36**, 94–99.
9. Cong,Y.S., Wright,W.E. and Shay,J.W. (2002) Human telomerase and its regulation. *Microbiol. Mol. Biol. Rev.*, **66**, 407–425.
10. Ye,J.Z., Donigian,J.R., van Overbeek,M., Loayza,D., Luo,Y., Krutchinsky,A.N., Chait,B.T. and de Lange,T. (2004) TIN2 binds TRF1 and TRF2 simultaneously and stabilizes the TRF2 complex on telomeres. *J. Biol. Chem.*, **279**, 47264–47271.
11. Liu,D., O'Connor,M.S., Qin,J. and Songyang,Z. (2004) Telosome, a mammalian telomere-associated complex formed by multiple telomeric proteins. *J. Biol. Chem.*, **279**, 51338–51342.
12. de Lange,T. (2005) Shelterin: the protein complex that shapes and safeguards human telomeres. *Genes Dev.*, **19**, 2100–2110.
13. Karlseder,J., Broccoli,D., Dai,Y., Hardy,S. and de Lange,T. (1999) p53- and ATM-dependent apoptosis induced by telomeres lacking TRF2. *Science*, **283**, 1321–1325.
14. van Steensel,B., Smogorzewska,A. and de Lange,T. (1998) TRF2 protects human telomeres from end-to-end fusions. *Cell*, **92**, 401–413.

15. Karlseder,J., Smogorzewska,A. and de Lange,T. (2002) Senescence induced by altered telomere state, not telomere loss. *Science*, **295**, 2446–2449.

16. Griffith,J.D., Comeau,L., Rosenfield,S., Stansel,R.M., Bianchi,A., Moss,H. and de Lange,T. (1999) Mammalian telomeres end in a large duplex loop. *Cell*, **97**, 503–514.

17. Stansel,R.M., de Lange,T. and Griffith,J.D. (2001) T-loop assembly *in vitro* involves binding of TRF2 near the 3′ telomeric overhang. *EMBO J.*, **20**, 5532–5540.

18. Yoshimura,S.H., Maruyama,H., Ishikawa,F., Ohki,R. and Takeyasu,K. (2004) Molecular mechanisms of DNA end-loop formation by TRF2. *Genes Cells*, **9**, 205–218.

19. Court,R., Chapman,L., Fairall,L. and Rhodes,D. (2005) How the human telomeric proteins TRF1 and TRF2 recognize telomeric DNA: a view from high-resolution crystal structures. *EMBO Rep.*, **6**, 39–45.

20. Konishi,A. and de Lange,T. (2008) Cell cycle control of telomere protection and NHEJ revealed by a ts mutation in the DNA-binding domain of TRF2. *Genes Dev.*, **22**, 1221–1230.

21. Nikitina,T. and Woodcock,C.L. (2004) Closed chromatin loops at the ends of chromosomes. *J. Cell Biol.*, **166**, 161–165.

22. Rossetti,L., Cacchione,S., De Menna,A., Chapman,L., Rhodes,D. and Savino,M. (2001) Specific interactions of the telomeric protein Rap1p with nucleosomal binding sites. *J. Mol. Biol.*, **306**, 903–913.

23. Galati,A., Rossetti,L., Pisano,S., Chapman,L., Rhodes,D., Savino,M. and Cacchione,S. (2006) The human telomeric protein TRF1 specifically recognizes nucleosomal binding sites and alters nucleosome structure. *J. Mol. Biol.*, **360**, 377–385.

24. Fletcher,T.M., Krishnan,U., Serwer,P. and Hansen,J.C. (1994) Quantitative agarose gel electrophoresis of chromatin: nucleosome-dependent changes in charge, sharp, and deformability at low ionic strength. *Biochemistry*, **33**, 2226–2233.

25. Hansen,J.C., Fletcher,T.M. and Kreider,J.I. (1999) Quantitative analysis of chromatin higher-order organization using agarose gel electrophoresis. *Methods Mol. Biol.*, **119**, 113–125.

26. Fletcher,T.M., Serwer,P. and Hansen,J.C. (1994) Quantitative analysis of macromolecular conformational changes using agarose gel electrophoresis: application to chromatin folding. *Biochemistry*, **33**, 10859–10863.

27. Fletcher,T.M. and Hansen,J.C. (1995) Core histone tail domains mediate oligonucleosome folding and nucleosomal DNA organization through distinct molecular mechanisms. *J. Biol. Chem.*, **270**, 25359–25362.

28. Tse,C., Fletcher,T.M. and Hansen,J.C. (1998) Enhanced transcription factor access to arrays of histone H3/H4 tetramer.DNA complexes *in vitro*: implications for replication and transcription. *Proc. Natl Acad. Sci. USA*, **95**, 12169–12173.

29. Carruthers,L.M., Bednar,J., Woodcock,C.L. and Hansen,J.C. (1998) Linker histones stabilize the intrinsic salt-dependent folding of nucleosomal arrays: mechanistic ramifications for higher-order chromatin folding. *Biochemistry*, **37**, 14776–14787.

30. Georgel,P.T., Fletcher,T.M., Hager,G.L. and Hansen,J.C. (2003) Formation of higher-order secondary and tertiary chromatin structures by genomic mouse mammary tumor virus promoters. *Genes Dev.*, **17**, 1617–1629.

31. Amiard,S., Doudeau,M., Pinte,S., Poulet,A., Lenain,C., Faivre-Moskalenko,C., Angelov,D., Hug,N., Vindigni,A., Bouvet,P. *et al.* (2007) A topological mechanism for TRF2-enhanced strand invasion. *Nat. Struct. Mol. Biol.*, **14**, 147–154.

32. Hansen,J.C., Ausio,J., Stanik,V.H. and van Holde,K.E. (1989) Homogeneous reconstituted oligonucleosomes, evidence for salt-dependent folding in the absence of histone H1. *Biochemistry*, **28**, 9129–9136.

33. Khan,S.J., Yanez,G., Seldeen,K., Wang,H., Lindsay,S.M. and Fletcher,T.M. (2007) Interactions of TRF2 with model telomeric ends. *Biochem. Biophys. Res. Commun.*, **363**, 44–50.

34. Yanez,G.H., Khan,S.J., Locovei,A.M., Pedroso,I.M. and Fletcher,T.M. (2005) DNA structure-dependent recruitment of telomeric proteins to single-stranded/double-stranded DNA junctions. *Biochem. Biophys. Res. Commun.*, **328**, 49–56.

35. Côté,J., Utley,R.T. and Workman,J.L. (1995) Basic analysis of transcription factor binding to nucleosomes. *Methods Mol. Genet.*, **6**, 108–128.

36. Stein,A., Whitlock,J.P. Jr. and Bina,M. (1979) Acidic polypeptides can assemble both histones and chromatin *in vitro* at physiological ionic strength. *Proc. Natl Acad. Sci. USA*, **76**, 5000–5004.

37. Pfaffle,P., Gerlach,V., Bunzel,L. and Jackson,V. (1990) *In vitro* evidence that transcription-induced stress causes nucleosome dissolution and regeneration. *J. Biol. Chem.*, **265**, 16830–16840.

38. Steger,D.J., Owen-Hughes,T., John,S. and Workman,J.L. (1997) Analysis of transcription factor-mediated remodeling of nucleosomal arrays in a purified system. *Methods*, **12**, 276–285.

39. Griess,G.A., Moreno,E.T., Easom,R.A. and Serwer,P. (1989) The sieving of spheres during agarose gel electrophoresis: quantitation and modeling. *Biopolymers*, **28**, 1475–1484.

40. Wang,H., Bash,R., Yodh,J.G., Hager,G.H., Lohr,D. and Lindsay,S.M. (2002) Glutaraldehyde modified mica: a new surface for atomic force microscopy of chromatin. *Biophys. J.*, **83**, 3619–3625.

41. Pedroso,I.M., Hayward,W. and Fletcher,T.M. (2009) The effect of the TRF2 N-terminal and TRFH regions on telomeric G-quadruplex structures. *Nucleic Acids Res.*, **37**, 1541–1554.

42. Cacchione,S., Cerone,M.A. and Savino,M. (1997) *In vitro* low propensity to form nucleosomes of four telomeric sequences. *FEBS Lett.*, **400**, 37–41.

43. Rossetti,L., Cacchione,S., Fua,M. and Savino,M. (1998) Nucleosome assembly on telomeric sequences. *Biochemistry*, **37**, 6727–6737.

44. Luger,K., Mäder,A.W., Richmond,R.K., Sargent,D.F. and Richmond,T.J. (1997) Crystal structure of the nucleosome core particle at 2.8 A resolution. *Nature*, **389**, 251–260.

45. Arents,G. and Moudrianakis,E.N. (1993) Topography of the histone octamer surface: repeating structural motifs utilized in the docking of nucleosomal DNA. *Proc. Natl Acad. Sci. USA*, **90**, 10489–10493.

46. Simpson,R.T., Thoma,F. and Brubaker,J.M. (1985) Chromatin reconstituted from tandemly repeated cloned DNA fragments and core histones: a model system for study of higher order structure. *Cell*, **42**, 799–808.

47. Lohr,D., Bash,R., Wang,H., Yodh,J. and Lindsay,S. (2007) Using atomic force microscopy to study chromatin structure and nucleosome remodeling. *Methods*, **41**, 333–341.

48. Hanaoka,S., Nagadoi,A. and Nishimura,Y. (2005) Comparison between TRF2 and TRF1 of their telomeric DNA-bound structures and DNA-binding activities. *Protein Sci.*, **14**, 119–130.

49. Lumpkin,O.J., Dejardin,P. and Zimm,B.H. (1985) Theory of gel electrophoresis of DNA. *Biopolymers*, **24**, 1573–1593.

50. Slater,G.W., Rousseau,J. and Noolandi,J. (1987) On the stretching of DNA in the reptation theories of gel electrophoresis. *Biopolymers*, **26**, 863–872.

51. Noolandi,J. (1992) Polymer dynamics in electrophoresis of DNA. *Annu. Rev. Phys. Chem.*, **43**, 237–256.

52. Verdun,R.E. and Karlseder,J. (2006) The DNA damage machinery and homologous recombination pathway act consecutively to protect human telomeres. *Cell*, **127**, 709–720.

53. Boyer,L.A., Langer,M.R., Crowley,K.A., Tan,S., Denu,J.M. and Peterson,C.L. (2002) Essential role for the SANT domain in the functioning of multiple chromatin remodeling enzymes. *Mol. Cell.*, **10**, 935–942.

54. Grune,T., Brzeski,J., Eberharter,A., Clapier,C.R., Corona,D.F., Becker,P.B. and Muller,C.W. (2003) Crystal structure and functional analysis of a nucleosome recognition module of the remodeling factor ISWI. *Mol. Cell*, **12**, 449–460.

55. Clapier,C.R., Langst,G., Corona,D.F., Becker,P.B. and Nightingale,K.P. (2001) Critical role for the histone H4 N terminus in nucleosome remodeling by ISWI. *Mol. Cell Biol.*, **21**, 875–883.

56. Mo,X., Kowenz-Leutz,E., Laumonnier,Y., Xu,H. and Leutz,A. (2005) Histone H3 tail positioning and acetylation by the c-Myb but not the v-Myb DNA-binding SANT domain. *Genes Dev.*, **19**, 2447–2457.

57. Pisano,S., Marchioni,E., Galati,A., Mechelli,R., Savino,M. and Cacchione,S. (2007) Telomeric nucleosomes are intrinsically mobile. *J. Mol. Biol.*, **369**, 1153–1162.

58. Benetti,R., Schoeftner,S., Munoz,P. and Blasco,M.A. (2008) Role of TRF2 in the assembly of telomeric chromatin. *Cell Cycle*, **7**, 3461–3468.